Arginine-selective modulation of the lysosomal transporter PQLC2 through a gate-tuning mechanism

Xavier Leray[a,1], Rossella Conti[a], Yan Li[b], Cécile Debacker[a], Florence Castelli[c], François Fenaille[c], Anselm A. Zdebik[b], Michael Pusch[d], and Bruno Gasnier[a,2]

[a]Saints-Pères Paris Institute for the Neurosciences, Université de Paris, Centre National de la Recherche Scientifique, F-75006 Paris, France; [b]Department of Neuroscience, Physiology and Pharmacology, University College London Medical School, London NW3 2PF, United Kingdom; [c]Département Médicaments et Technologies pour la Santé, Université Paris-Saclay, Commissariat à l'Énergie Atomique et aux Énergies Alternatives, Institut National de Recherche pour l'Agriculture, l'Alimentation et l'Environnement, F-91191 Gif sur Yvette, France; and [d]Istituto di Biofisica, Consiglio Nazionale delle Richerche, 16149 Genova, Italy

Edited by Robert H. Edwards, University of California, San Francisco, CA, and approved June 21, 2021 (received for review December 21, 2020)

Lysosomes degrade excess or damaged cellular components and recycle their building blocks through membrane transporters. They also act as nutrient-sensing signaling hubs to coordinate cell responses. The membrane protein PQ-loop repeat-containing protein 2 (PQLC2; "picklock two") is implicated in both functions, as it exports cationic amino acids from lysosomes and serves as a receptor and amino acid sensor to recruit the C9orf72/SMCR8/WDR41 complex to lysosomes upon nutrient starvation. Its transport activity is essential for drug treatment of the rare disease cystinosis. Here, we quantitatively studied PQLC2 transport activity using electrophysiological and biochemical methods. Charge/substrate ratio, intracellular pH, and reversal potential measurements showed that it operates in a uniporter mode. Thus, PQLC2 is uncoupled from the steep lysosomal proton gradient, unlike many lysosomal transporters, enabling bidirectional cationic amino acid transport across the organelle membrane. Surprisingly, the specific presence of arginine, but not other substrates (lysine, histidine), in the discharge ("*trans*") compartment impaired PQLC2 transport. Kinetic modeling of the uniport cycle recapitulated the paradoxical substrate-yet-inhibitor behavior of arginine, assuming that bound arginine facilitates closing of the transporter's cytosolic gate. Arginine binding may thus tune PQLC2 gating to control its conformation, suggesting a potential mechanism for nutrient signaling by PQLC2 to its interaction partners.

lysosome | transporter | arginine-sensing | gating | PQLC2

Lysosomes maintain cells and tissues by degrading unwanted macromolecules, aggregates, organelles, and cell debris through endocytosis, phagocytosis, and autophagy. The building blocks released by lysosomal hydrolysis are exported to the cytosol by membrane transporters for reuse in biosynthetic pathways. A transcriptional feedback loop regulates lysosomal biogenesis and autophagy genes to adapt this degradative pathway to cellular needs (1). Lysosomal degradation also provides a route to acquire nutrients from extracellular macromolecules when free nutrients are scarce in the environment (2, 3). Besides these catabolic roles, lysosomes also constitute signaling hubs which integrate environmental and intracellular cues to control protein synthesis, anabolic pathways, and autophagy through the mechanistic target of rapamycin complex 1 (mTORC1) pathway. Intracellular amino acids activate Rag GTPases to recruit mTORC1 to lysosomes, where it is activated by the Rheb GTPase in response to nucleotide levels, oxygen, energy status, and growth factors (4, 5).

Amino acid sensing by mTORC1 involves cytosolic and lysosomal membrane proteins, which recognize specific amino acids or their metabolites. Leucine, a key activator of mTORC1, is sensed in the cytosol by Sestrin2 with micromolar affinity (half maximal effective concentration, EC_{50} = ~20 μM). Upon leucine binding, Sestrin2 dissociates from, and activates, GATOR2, a positive regulator of mTORC1 (6). Methionine is sensed through its metabolite, S-adenosylmethionine by SAMTOR, another cytosolic sensor. In its absence, SAMTOR activates GATOR1 to inhibit mTORC1. S-adenosylmethionine binding disrupts the interaction of SAMTOR with GATOR1 and its lysosomal scaffold KICSTOR, thus suppressing the inhibition of mTORC1 (4).

Arginine (Arg), another key activator of mTORC1, is sensed in the cytosol, but also in the lysosomal lumen, by distinct sensors. In the cytosol, CASTOR1 homodimers and CASTOR1–CASTOR2 heterodimers bind Arg with micromolar affinity (EC_{50} = ~25 μM) to dissociate from, and activate, GATOR2 (6). Arg is also sensed by the lysosomal membrane protein SNAT9, also known as SLC38A9, which has a dual function: it is a lysosomal exporter of essential amino acids gated by luminal Arg (3) and it acts as an Arg and cholesterol sensor to activate RagA/B-C/D heterodimers, and hence mTORC1, by stimulating the GTPase activity of the folliculin–FNIP2 complex toward RagC (7–11). Arg stimulates both SNAT9 activities in the high micromolar range (EC_{50} = 100 to 200 μM). As its central cavity is able to bind Arg in the cytosol-facing conformation (12), SNAT9 might sense both luminal and cytosolic Arg to activate mTORC1.

SNAT9 has a very low transport activity for Arg (3). The primary lysosomal transporter for Arg, along with other cationic

Significance

Lysosomes degrade and recycle cell components and integrate environmental and intracellular cues to regulate cell growth, metabolism, and autophagy. The lysosomal transporter PQLC2 exports cationic amino acids from lysosomes, and under amino acid starvation, it recruits to lysosomes a signaling complex implicated in neurological diseases. In this study, we show that PQLC2 transport activity is uncoupled from the lysosomal pH gradient and other ion gradients and that it is selectively modulated by arginine through a *trans*-inhibition mechanism. Kinetic modeling suggests that arginine accelerates the closing of its cytosolic gate. We propose a signaling model in which PQLC2 transduces the nutrient status to its cognate complex through opposing effects of lysosomal membrane potential and cytosolic arginine on its conformational state.

Author contributions: X.L., A.A.Z., and B.G. designed research; X.L., R.C., Y.L., C.D., F.C., A.A.Z., and B.G. performed research; M.P. contributed new reagents/analytic tools; X.L., R.C., Y.L., F.C., F.F., A.A.Z., M.P., and B.G. analyzed data; and X.L. and B.G. wrote the paper.

The authors declare no competing interest.

This article is a PNAS Direct Submission.

See online for related content such as Commentaries.

[1]Present address: Laboratoire Signalisation Fonctionnelle des Canaux Ioniques et Récepteurs, Université d'Angers, Institut National de Recherche pour l'Agriculture, l'Alimentation et l'Environnement, 49045 Angers, France.

[2]To whom correspondence may be addressed. Email: bruno.gasnier@u-paris.fr.

This article contains supporting information online at https://www.pnas.org/lookup/suppl/doi:10.1073/pnas.2025315118/-/DCSupplemental.

Published August 3, 2021.

amino acids (CAA), has been identified as the PQ-loop repeat-containing protein 2 (PQLC2; pronounced "picklock two" for convenience) (13, 14), encoded by the SLC66A1 gene (15). PQLC2 belongs to the PQ-loop protein family (Pfam no. PF04193) characterized by the presence of seven transmembrane helices and a duplicated motif with a highly conserved proline–glutamine dipeptide. Its founding member, cystinosin, is an H^+-coupled lysosomal cystine transporter defective in human cystinosis (16–18). These amino acid transporters are distantly related to the SWEET and SemiSWEET sugar transporters, the mitochondrial pyruvate carrier, and the KDEL receptor (19, 20).

As SNAT9, PQLC2 has a dual role in amino acid recycling and amino acid signaling at the lysosomal membrane. It selectively exports Arg, Lys, and His from the lysosomal lumen (13, 14). This transport activity is essential for the cysteamine therapy of cystinosis because it provides a salvage pathway to deplete lysosomal cystine by exporting a lysine-like cysteamine–cysteine mixed disulfide from the lysosomal lumen (13, 14). On the other hand, PQLC2 acts as a lysosomal receptor that recruits the C9orf72-SMCR8-WDR41 (CSW) complex to lysosomes under CAA starvation (21). In *Caenorhabditis elegans*, the PQLC2 ortholog LAAT-1 decreases sensitivity to endoplasmic reticulum stress. This role apparently involves its amino acid transport activity rather than amino acid sensing because CAA supplementation rescues the phenotype of *laat-1* mutants (22).

The CSW complex is involved in autophagy, lysosome biogenesis, phagosome maturation, actin dynamics, and down-regulation of Toll-like receptors (5, 23–26), and its dysfunction is implicated in frontotemporal degeneration and amyotrophic lateral sclerosis (5, 26). Recent studies showed that it acts as a GTPase-activating protein toward a specific set of small GTPases, including Arf1, Arf5, Arf6, Rab8a, and Rab11a (27, 28) and that it associates with lysosomes under amino acid starvation through an interaction between its WDR41 subunit and PQLC2 (21).

In this study, we characterized the ion and voltage dependence of PQLC2 transport activity using electrophysiology. In the course of this study, we discovered a specific modulation of the PQLC2 current by Arg but not other substrates (Lys, His). An investigation of the underlying mechanism using electrophysiology and kinetic modeling identified a specific effect of Arg on PQLC2 gating as the most plausible explanation. This mechanism suggests in turn a hypothetical model for the amino acid signaling function of PQLC2.

Results

PQLC2 Is a Cationic Amino Acid Uniporter. To examine the ion-coupling properties of PQLC2, we first measured its charge/substrate ratio by applying tritiated arginine ([^{3}H]Arg) to voltage-clamped oocytes expressing PQLC2-LL290/291AA-EGFP at the plasma membrane (hereafter referred to as PQLC2 oocytes). Experiments were done at pH 5.0 to mimic the acidic lumen of the lysosome and to activate PQLC2 (14). The time integral of the evoked current was proportional to the amount of accumulated [^{3}H]Arg (Fig. 1*A*), with a slope of 0.94 positive elementary charge per cationic Arg molecule (R^2 = 0.96, n = 18 oocytes). Thus, if PQLC2 transports inorganic ions together with Arg, their contribution to the charge flux should compensate each other.

We next asked whether PQLC2 is coupled to protons like many lysosomal transporters (2, 17, 29). The internal pH (pH_{in}) of PQLC2 oocytes was monitored under voltage clamp with a pH-sensitive fluorescent probe (BCECF) or an H^+-selective electrode. Applications of Arg or Lys at pH_{out} 6.0 or 5.0 induced robust currents but did not detectably alter pH_{in}. In contrast, the application of His acidified PQLC2 oocytes (Fig. 1*B* and *SI Appendix*, Fig. S1 *A*, *B*, *D*, and *E*). The acidification rate was proportional to the His current above a threshold of 131 ± 26 nA (n = 5; Fig. 1*C* and *SI Appendix*, Fig. S1 *D* and *F*). As His has a lower side chain pK_a (6.0) than Lys and Arg (10.5 and 12.5, respectively), this

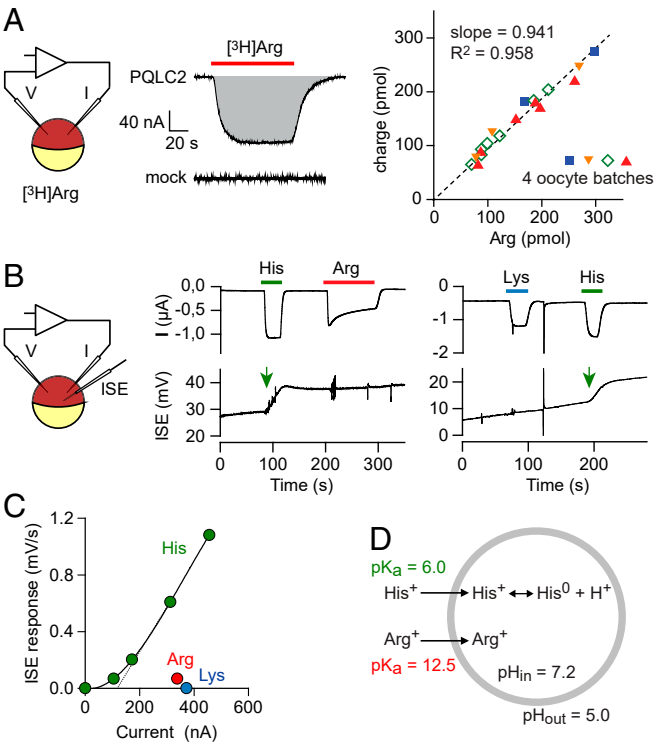

Fig. 1. PQLC2 is not driven by protons. (*A*) Charge–substrate ratio measurements. Representative current traces elicited by [^{3}H]Arg in a PQLC2 oocyte and a negative control. The accumulated charge (shaded area) is proportional to accumulated Arg with a slope of 0.94 elementary charge per molecule. (*B* and *C*) Intracellular pH measurements with an ion-selective electrode (ISE). His (arrows), but not Arg or Lys, applied to PQLC2 oocytes at pH 5.0 induces an intracellular acidification. The graph in *C* shows a representative example of the acidification/current relationship. (*D*) Model for the His-induced acidification.

cytosolic acidification must reflect the release of protons from cationic His molecules imported by PQLC2 (Fig. 1*D*). In agreement with this model, canavanine, another PQLC2 substrate (14) with a low side chain pK_a (7.0; oxyguanidinium group), acidified PQLC2 oocytes (*SI Appendix*, Fig. S1*C*). Therefore, PQLC2 is not coupled to protons. Its activation at low luminal (extracellular) pH (14) reflects a kinetic, but not a thermodynamic, effect.

Finally, we examined the possibility that ions other than protons drive PQLC2 transport. As we had noticed that PQLC2 oocytes substantially accumulate CAAs during current measurements (see next section), we took advantage of this effect to measure PQLC2 reversal potentials (V_{rev}). PQLC2 oocytes were perfused for 5 to 15 min with 20 mM Lys or Arg to increase their internal CAA concentration ($[CAA]_{in}$) and immediately afterward were subjected to voltage jumps at varying external CAA concentrations ($[CAA]_{out}$) to determine V_{rev} (Fig. 2 *A* and *B*). A stable $[CAA]_{in}$ level was maintained throughout the experiment (Fig. 2*C*, purple dot). V_{rev} values varied linearly with $\log([Lys]_{out})$ and $\log([Arg]_{out})$ with mean slopes of 52 ± 2 (± SEM; n = 6 oocytes) and 57 ± 3 mV/decade (n = 8), respectively (Fig. 2 *C* and *D*). The PQLC2 cycle is thus thermodynamically coupled with the transfer of one positive elementary charge per CAA molecule. To test whether PQLC2 is coupled to inorganic ions, we changed $[Na^+]_{out}$, $[K^+]_{out}$, $[Cl^-]_{out}$, and pH_{out} by one to two order of magnitudes and examined the impact on V_{rev}. None of these conditions altered V_{rev} (Fig. 2*E*), excluding these ions from the transport cycle.

Altogether, these data indicate that PQLC2 is a CAA uniporter or a CAA channel. As PQLC2 contains conserved PQ

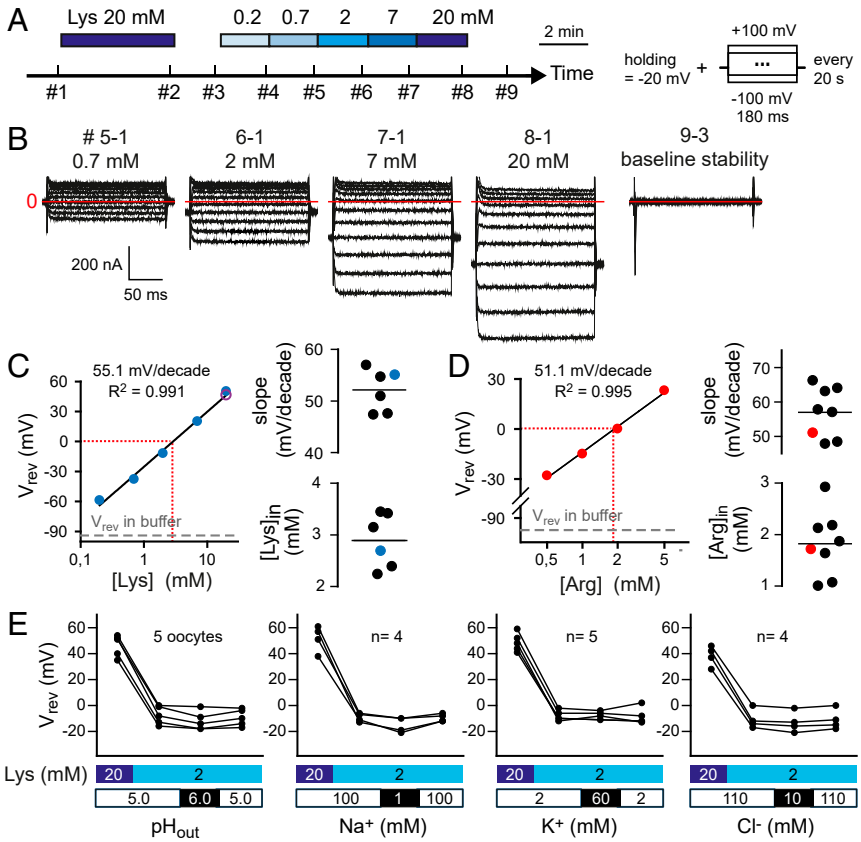

Fig. 2. PQLC2 is a cationic amino acid uniporter. (*A*) Protocol used for reversal potential measurements. After accumulating Lys through PQLC2, the oocyte is equilibrated with varying Lys_{out} concentrations and subjected to voltage jumps. (*B*) Representative Lys-evoked current traces, obtained by subtracting the raw currents recorded at the numbered tick marks on the time's arrow in *A*. (*C*) Lys_{out} dependence of V_{rev} for the oocyte shown in *B* (blue dots) and five other PQLC2 oocytes. V_{rev} is proportional to log($[Lys]_{out}$) with a mean slope 52 ± 2 mV/decade, consistent with the translocation of one elementary charge per Lys molecule. The internal Lys concentration is deduced from this relationship (red dotted line). The value of V_{rev} at the end of the Lys-loading phase (open purple dot) shows that a constant $[Lys]_{in}$ was maintained throughout the experiment. (*D*) V_{rev} measurements obtained with Arg as substrate. (*E*) V_{rev} is not affected by 10- to 100-fold changes in the external concentrations of H^+, Na^+, K^+, and Cl^-.

motifs which are critical for alternating-access transitions in related SemiSWEET transporters (30), a channel mechanism is unlikely.

Luminal Arg Inwardly Rectifies the PQLC2 Current. We next examined the voltage dependence of the transport current for various substrates. Intriguingly, first studies of Arg transport yielded inconsistent current–voltage (I–V) curves with a large, variable, paradoxical inward current at positive potentials in apparent contradiction with the uniport mechanism. This paradox could be solved when I–V curve measurements were initiated before any exposure of PQLC2 oocytes to exogenous CAAs ("naive" oocytes), allowing to define a background current subtraction procedure that is not influenced by substrate accumulation inside the oocytes (see next paragraph).

Representative current traces of a naive PQLC2 oocyte perfused twice with 20 mM Lys are shown in Fig. 3 *A*, *C*, and *F*. The first application evoked an inward current at negative potential, as expected. Surprisingly, an outward current was also induced at positive potential. This response could be assigned to the efflux of Lys_{in} accumulated during Lys perfusion based on the following evidence: 1) the outward current persisted, and increased, after washing out Lys from the bath (Fig. 3 *A* and *F*); 2) it correlated with the PQLC2 expression level (*SI Appendix*, Fig. S2*C*); and 3) amino acid measurements confirmed the rise of $[Lys]_{in}$ well above its endogenous level after a single Lys application (Fig. 3*E*). When Lys was applied again, the outward current seemed to vanish when we used a classical subtraction to extract the PQLC2 current (4 – 3 subtraction in Fig. 3 *A* and *C*). However, this procedure is inappropriate after the first application because the background current recorded in wash buffer now comprises a Lys_{in}-evoked PQLC2 component. To isolate the actual PQLC2 current, we defined a subtraction procedure in which the background current recorded in the initial naive state ($[Lys]_{in}$ at minimal, endogenous level) is subtracted to all subsequent applications (4 – 1 subtraction in Fig. 3 *A* and *C*). The recordings analyzed with this procedure yielded consistent I–V curves with a leftward shift on the second application reflecting the increase in $[Lys]_{in}$ (Fig. 3 *C*, *Right*, and *SI Appendix*, Fig. S2*D*). The Lys I–V curves showed an inward rectification consistent with the lower value of $[Lys]_{in}$ (Fig. 2*C*) relative to $[Lys]_{out}$ in these experiments (see the patch-clamp experiments in Fig. 3*I* for the virtual absence of rectification of the Lys-evoked current when $[Lys]_{in} = [Lys]_{out}$).

We next used this approach to characterize the Arg current. PQLC2 oocytes substantially accumulate Arg-like Lys since an outward current correlating with the PQLC2 expression level is observed after washing out Arg from the bath (Fig. 3 *B* and *G* and *SI Appendix*, Fig. S2*C*). However, in contrast with Lys, this outward current is suppressed during Arg application (compare 3 – 1 and 4 – 1 subtractions in Fig. 3 *A* and *B* and see also raw traces in *SI Appendix*, Fig. S2*A*). In other terms, extracellular/luminal Arg strongly reduces electrogenic PQLC2 transport from the cytosol to the extracellular/luminal side, that is, Arg effectively transinhibits the uniport activity. In the next Arg application, this

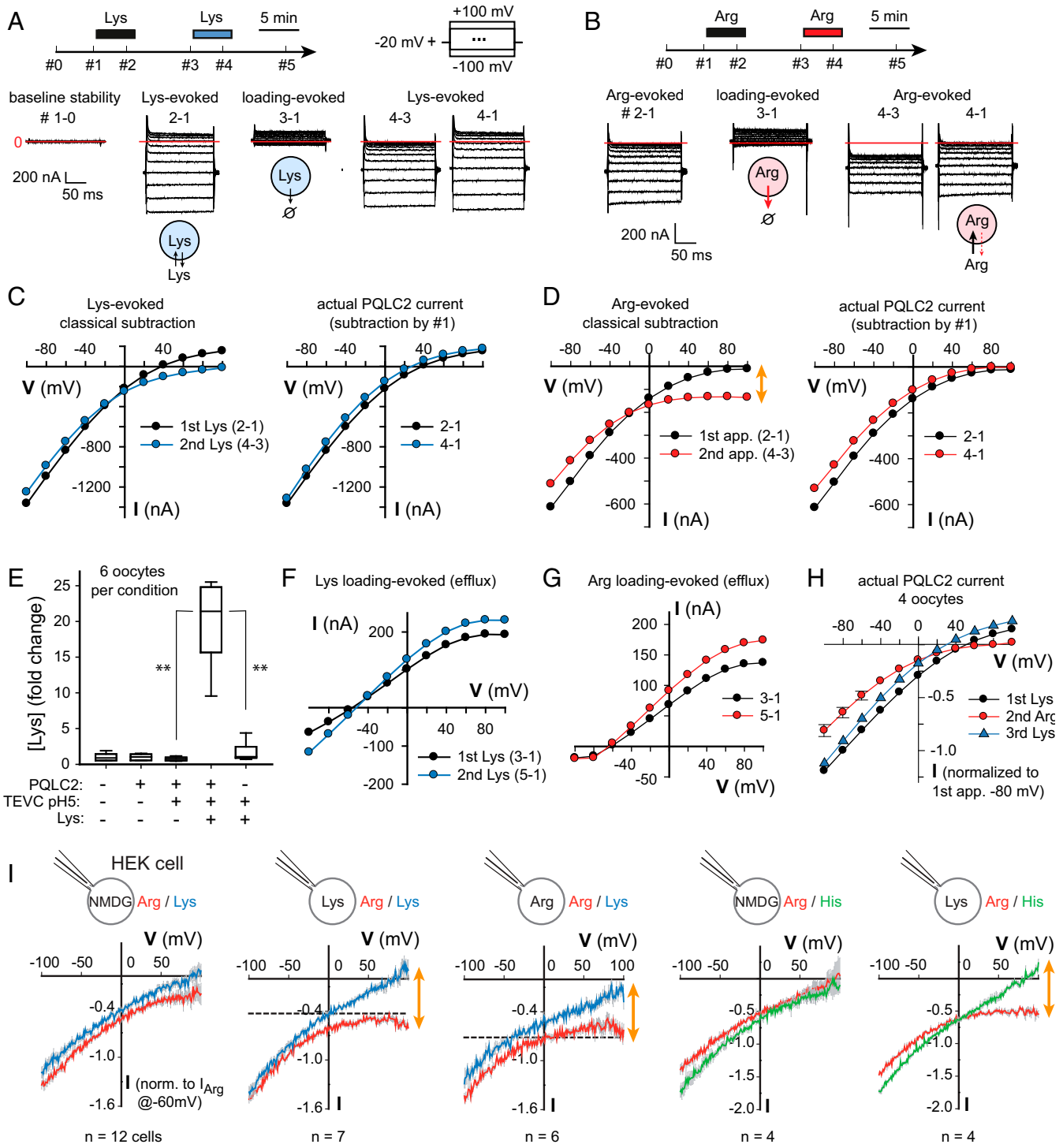

Fig. 3. Arg_{out} inwardly rectifies the PQLC2 current. (*A–D*) Voltage dependence of the Lys and Arg currents. Naive PQLC2 oocytes were perfused twice with either 20 mM Lys or 20 mM Arg and subjected to voltage jumps every 20 s. Representative PQLC2 current traces in *A* and *B* were obtained by subtracting the raw current recorded at the corresponding tick marks on the time's arrow. With Arg, the outward current observed during the wash steps (3 – 1 subtraction) is fully suppressed by the presence of Arg in the bath (2 – 1 and 4 – 1 subtractions). *C* and *D* show the corresponding I–V curves during substrate application. In each panel, two subtraction procedures are compared. (*Left*) The result of the classical subtraction procedure, which induces an artifact during the second application of Arg (double arrow), reflecting the suppression of the outward current by Arg_{out}. (*Right*) The actual PQLC2 current. (*E*) Oocytes were perfused 5 min with 20 mM, Lys and their Lys content was measured by liquid chromatography coupled to high-resolution mass spectrometry (LC–HRMS). $^{**}P \leq 0.002$. (*F* and *G*) I–V curves of the PQLC2 current recorded during the wash steps of the oocytes shown in *A* and *B*. The outward current reflects the efflux of accumulated Lys or Arg molecules. Its shift to an inward current at negative potential may reflect the reentry of Lys or Arg molecules leaving the oocyte at holding potential. (*H*) Mean I–V curves of four oocytes successively perfused with 20 mM Lys, Arg, and Lys again. (*I*) Whole-cell patch-clamp recording of PQLC2 in HEK cells. The mean current ± SEM (gray shading) evoked by 20 mM CAA_{out} is plotted against voltage. CAA_{in} (20 mM) was delivered, or not (20 mM NMDG), through the patch-clamp pipette. In CAA-loaded cells, the actual PQLC2 current cannot be determined owing to the lack of zero-in, zero-out reference. The dashed line shows its expected zero value based on the null reversal potential in symmetrical conditions. The double arrows reflect the suppression of the PQLC2 outward current by extracellular Arg.

effect creates a subtraction artifact with the (improper) classical procedure (Fig. 3*D*, double arrow). The correct subtraction procedure avoids this artifact and yields consistent inwardly rectifying I–V curves with a leftward shift upon successive applications, reflecting the increase in Arg_{in} (Fig. 3*G* and *SI Appendix*, Fig. S2*D*).

The Lys and Arg currents of PQLC2 differ by their degree of inward rectification: the rectification becomes so strong with Arg that no outward current can be observed in the potential range analyzed. Successive applications of Lys and Arg showed that this effect selectively depends on Arg_{out}, regardless of the amino acid carrying the outward current (Fig. 3*H* and *SI Appendix*, Fig. S2*B*).

To determine the concentration dependence of this effect, we loaded PQLC2 oocytes with high levels of Lys or Arg (to minimize subsequent changes in $[Lys]_{in}$ or $[Arg]_{in}$) and characterized the PQLC2 I-V curves at varying $[Lys]_{out}$ or $[Arg]_{out}$, respectively. *SI Appendix*, Fig. S3 shows the dependence of PQLC2 currents on $[CAA]_{out}$ at −80 and +80 mV. The inward current recorded at −80 mV followed Michaelis–Menten kinetics (*SI Appendix*, Fig. S3 *A* and *C*) with a K_M of 7.3 and 1.7 mM for Lys_{out} and Arg_{out}, respectively. The outward current recorded at +80 mV decreased linearly in a gradual manner with Lys_{out}. In contrast, it decreased steeply in a hyperbolic manner with $[Arg]_{out}$ with a K_i of 3.2 mM, a value close to the K_M for Arg_{out} of the inward current (*SI Appendix*, Fig. S3 *B* and *C*).

To confirm the inward rectifying effect of Arg_{out} and rule out an artifact from the oocyte expression system, we recorded PQLC2 currents in whole-cell patch-clamped human embryonic kidney 293T (HEK293T) cells, a configuration allowing direct delivery of internal amino acids by dialysis from the micropipette solution. An application at pH_{out} 5.0 of 20 mM CAA_{out} to cells expressing PQLC2-LL290/291AA-EGFP at the plasma membrane ("PQLC2 cells") induced a robust inward current, which was not detected in mock cells (Fig. 3*I* and *SI Appendix*, Fig. S2 *E* and *F*). We applied voltage ramps to characterize the voltage dependence of this current. In the absence of internal amino acid (pipette filled with *N*-methyl-D-glucamine [NMDG] buffer), an application of 20 mM Lys_{out}, Arg_{out}, or His_{out} yielded nearly superimposable I–V curves. However, when 20 mM Lys_{in} or Arg_{in} was included in the pipette, the PQLC2 current evoked by Arg_{out}, but not Lys_{out} or His_{out}, showed a strong inward rectification (Fig. 3*I* and *SI Appendix*, Fig. S2 *E* and *G*) in agreement with the oocyte data.

In conclusion, Arg_{out} induces a selective inward rectification of the PQLC2 current, regardless of the amino acid carrying the current, in two expression systems. The concentration dependence of this effect (*SI Appendix*, Fig. S3 *B* and *C*) suggests that it involves Arg binding to the extracellular (luminal) side of the transporter.

Cytosolic Arg Reduces the PQLC2 Current. We next asked whether Arg could also modulate the PQLC2 current from the cytosolic side. We thus measured the PQLC2 current evoked by pulse applications of Lys before and after sustained oocyte loading with either Lys or Arg (Fig. 4*A*). If the two amino acids interact similarly with PQLC2 on the cytosolic side, the pulse current should be exclusively affected by the shallower CAA gradient across the oocyte membrane after CAA loading. In contrast with this prediction, Arg loading decreased the pulse current to a greater extent than Lys loading (34 ± 1% versus 78 ± 5% of first-pulse current, respectively; $n = 5$), although Arg_{in} (4.3 ± 0.2 mM) accumulated to lower levels than Lys_{in} (8.1 ± 0.4 mM) (Fig. 4 *B* and *C*). This Arg_{in}-selective reduction also manifested as a steep decrease of the loading current during the first minute of Arg, but not Lys, application (Fig. 4*A*, arrows). In agreement with the Lys pulse data, tail/peak ratios of 39 ± 4% and 71 ± 5% ($n = 5$) were measured for the Arg-loading and Lys-loading currents, respectively (Fig. 4*D*).

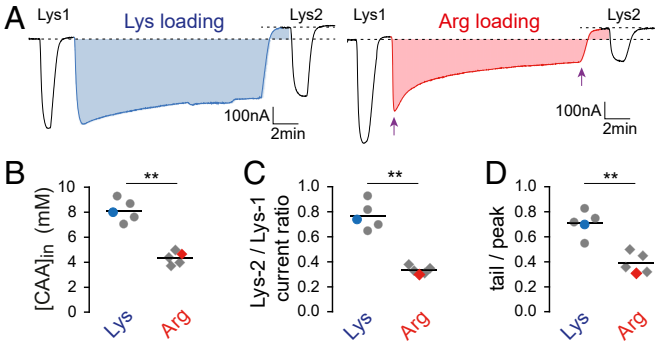

Fig. 4. Arg_{in} selectively reduces the inward current. Naive PQLC2 oocytes were perfused with a brief pulse of 20 mM Lys before and after sustained loading with 20 mM Lys or Arg at −60 mV. (*A*) Representative current traces. (*B*) Internal amino acid levels determined from the time integral of the loading currents based on an oocyte volume of 0.5 μL. (*C*) Ratio between the two pulse currents. (*D*) Current decrease during the loading step (arrows in *A*). The colored dots correspond to the oocytes shown in *A*. $^{**}P < 0.01$.

Arg_{in} thus selectively alters the PQLC2 inward current in a concentration range similar to the inhibition of the outward current by Arg_{out} (*SI Appendix*, Fig. S3 *B* and *C*). This selective effect of Arg in *trans* on both sides of PQLC2 suggests that it acts through the translocation pathway rather than through an Arg-selective allosteric site, although we cannot formally exclude the latter possibility.

Arginine Transinhibits PQLC2. Two potential mechanisms could account for the above data (Fig. 5*A*). First, the presence of Arg in *trans* (Arg_{trans}) could shift PQLC2 activity from an electrogenic uniport mode to an electroneutral CAA_{cis}/Arg_{trans} exchange mode undetected by electrophysiology. Alternately, Arg_{trans} could inhibit PQLC2 (uniport + exchange activities). To discriminate between these possibilities, we measured the charge/substrate ratio of PQLC2 in oocytes preloaded, or not, with either Lys or Arg. In the first hypothesis, Arg loading should selectively and substantially decrease this ratio, whereas in the second hypothesis, the ratio should not be affected (Fig. 5*A*). The outcome of these experiments is shown in Fig. 5*B*. While the charge/[^{3}H]Arg ratio of PQLC2 was 1.09 ± 0.04 ($n = 6$) in naive PQLC2 oocytes, it decreased to 0.90 ± 0.07 ($n = 11$) and 0.81 ± 0.04 ($n = 9$) in Lys- and Arg-loaded oocytes, respectively. The presence of CAA in *trans* therefore shifts 10 to 20% PQLC2 cycles from a uniport mode to an exchange mode. However, this shift is too small and nonselective to account for the PQLC2 current decrease by Arg_{in} (tail/peak ratio = 0.52 ± 0.04, $n = 9$). Moreover, these effects do not correlate (Fig. 5*C*). These data ruled out the exchange hypothesis, leaving Arg-induced *trans*-inhibition as the most likely mechanism.

To confirm this conclusion, we took advantage of the internal acidification induced by His uptake to measure the overall transport activity (uniport + exchange) of PQLC2 simultaneously with its uniport activity (His current). We thus recorded the intracellular acidification signals evoked by pulse applications of His under voltage clamp before and after oocyte loading with either Lys or Arg. Arg loading decreased the His-evoked acidification to a greater extent (post/pre-ratio = 0.36 ± 0.01, $n = 7$) than Lys loading (ratio = 0.72 ± 0.07, $n = 8$) (Fig. 5 *D* and *E*), in agreement with the decrease of the His current (post/pre-ratio = 0.39 ± 0.03 and 0.77 ± 0.03 for Arg and Lys, respectively) and of the loading current (tail/peak ratio = 0.53 ± 0.06 and 0.74 ± 0.03 for Arg and Lys, respectively). Altogether, these independent approaches show that Arg transinhibits PQLC2.

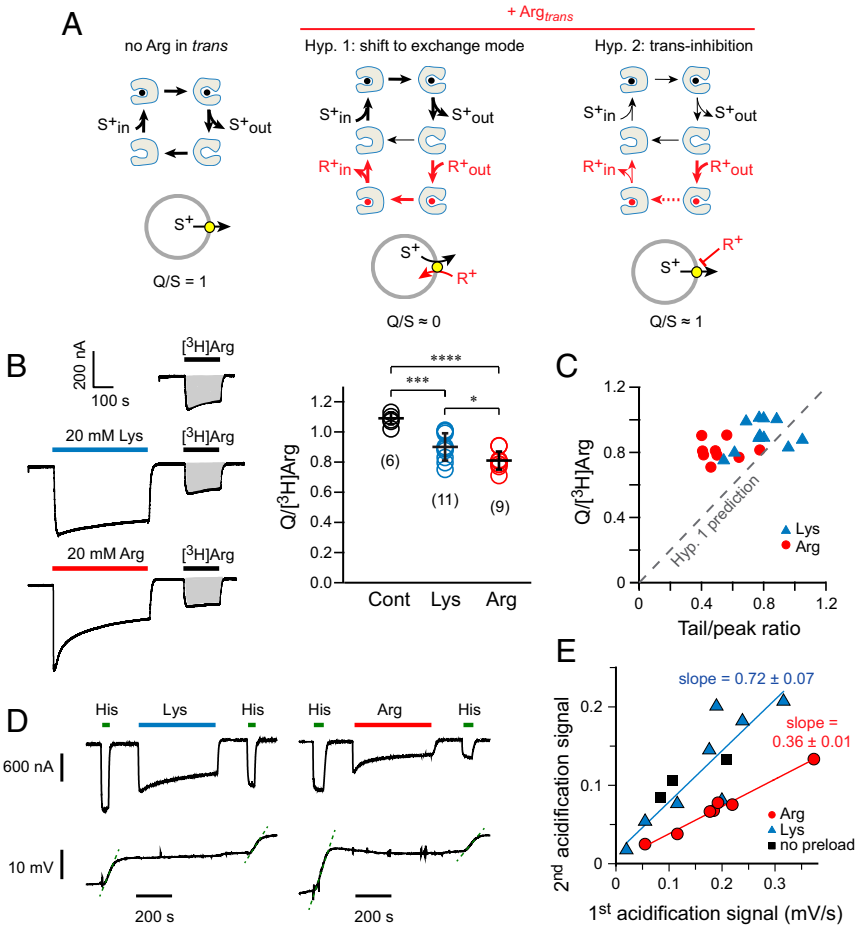

Fig. 5. Arginine transinhibits PQLC2. (*A*) Potential mechanisms for the Arg effect. The exchange and *trans*-inhibition mechanisms differentially alter the charge–substrate ratio (Q/S) of the transport cycle. (*B*) Charge–substrate ratio measurements in PQLC2 oocytes preloaded, or not, for ≥8 min at −60 mV with 20 mM Lys or Arg. Representative traces and mean ratio values for 6 to 11 oocytes per condition. *$P = 0.025$; ***$P \leq 0.001$; ****$P \leq 10^{-5}$. (*C*) The charge–substrate ratio is plotted against the PQLC2 current decrease during the loading step. (*D*) PQLC2 oocytes perfused with a brief pulse of His before and after sustained loading with either Lys or Arg were recorded with an intracellular H^+-selective electrode under voltage clamp. Representative current (*Top*) and pH electrode (*Bottom*) traces. The green dotted lines highlight the decreased acidification rate after Arg loading. (*E*) Relationship between the His-evoked acidification before and after Lys or Arg loading. The results are compared to those of PQLC2 oocytes without intervening loading steps (black squares).

Gate Kinetics Modulation by the Bound Substrate May Account for the Arg Properties. *Trans*-inhibition of membrane transporters by nontranslocated ligands (blockers) is a well-known phenomenon. However, the *trans*-inhibition of PQLC2 by Arg is paradoxical since the same compound is both a substrate in *cis* and an inhibitor in *trans*. Moreover, among three substrates (Lys, Arg, His), only one displays this dual behavior. To solve this paradox, we modeled the kinetics of PQLC2 and examined whether specific substrate/transporter interactions could induce Arg-like properties.

The kinetics and voltage dependence of PQLC2 were recapitulated in a six-state uniporter model comprising three conformations (lumen facing, occluded, and cytosol facing) in apo and loaded states (*SI Appendix*, Fig. S4*A*). Uniporter dynamics was explored using a Markov model software. After selecting a set of parameters mimicking the monotonic aspect of PQLC2 I–V curves (*SI Appendix*, Fig. S4*B* and Table S1), we studied the influence of substrate-dependent rate constants in a systematic manner. The gating constants in the loaded state ($k^S_{o.op}$, $k^S_{o.cl}$, $k^S_{i.op}$, and $k^S_{i.cl}$) were set to a low or high value (100 or 1,000 s^{-1} at 0 mV), yielding an array of 16 possibilities (Fig. 6*A*). One of the two remaining substrate-dependent constants, the dissociation rate on the luminal side ($k_{o.off}$; *SI Appendix*, Fig. S4*A*), was adjusted across the array to meet the principle of microscopic reversibility (equal clockwise and counterclockwise cycling at 0 mV when $[S^+]_{in} = [S^+]_{out}$). The dissociation rate from the cytosol-facing site ($k_{i.off}$) was kept unchanged ($K_{D.in} = 1$ mM). Apo-state rate constants were also kept unchanged. This systematic survey therefore compares 16 substrates interacting differently with the same uniporter.

Next, we simulated the I–V curves of these 16 substrates (20 mM out and 5 mM in) and searched for Arg-like properties based on the following: 1) the intensity of the outward current at +100 mV and 2) the effect of internal substrate on the inward current at −50 mV. The results are summarized as a heat map in Fig. 6*A*. Remarkably, only three substrates (no. 10, 11, and 12) mimicked the Arg behavior (low outward and inward currents in the tested conditions), and they share a common feature: a preference of the cytosolic (inner) gate for closure. We selected substrate no. 11 (S11), with a $K_{D.out}$ of 1 mM ($k_{o.off} = 10^{-6}$ s^{-1}), as an Arg-mimicking example for further studies. To select a "regular" (Lys/His-like) substrate, we relied on the fact that external Arg, Lys, and His evoke practically superimposable I–V curves in zero-*trans* condition (Fig. 3*I*, NMDG-containing cells). Substrate no. 3 (S3) was the only one matching S11 in this respect (*SI Appendix*, Fig. S4*C*), identifying these two substrates as a representative pair of Lys-like and Arg-like PQLC2 substrates. S11 differs from S3 by inducing faster closing of the cytosolic

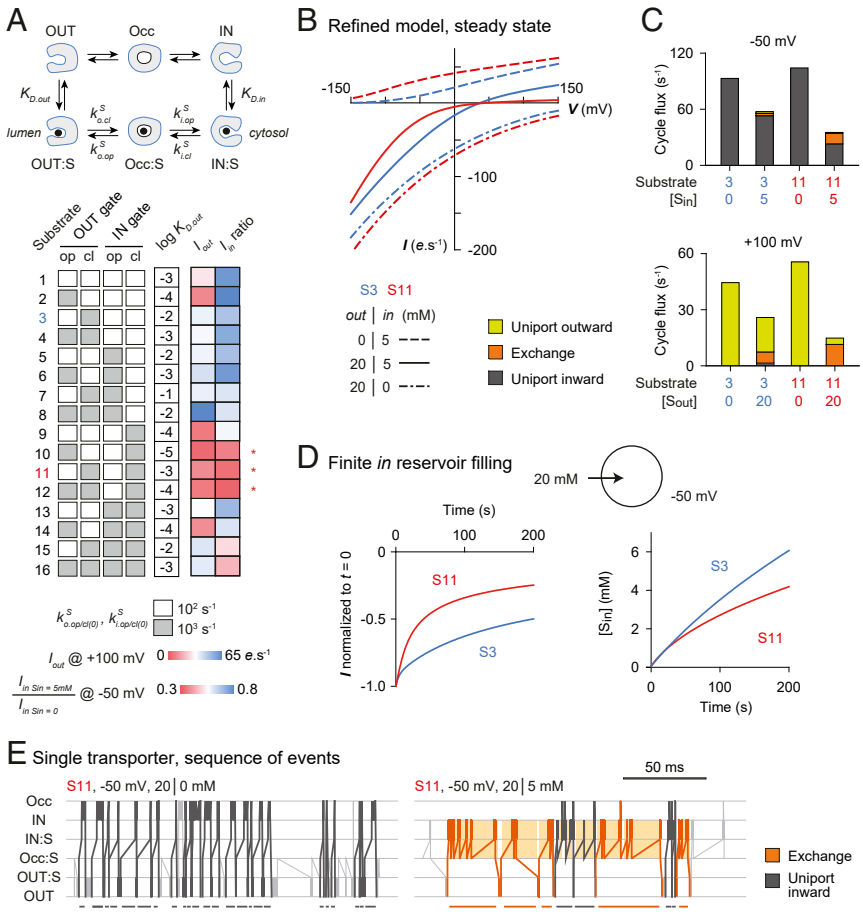

Fig. 6. Modulation of the transporter cytosolic gate by the bound substrate recapitulates the Arg-specific properties. (*A*) Systematic survey of substrate-specific parameters in a kinetic model of electrogenic uniporter. Gating constants of the loaded transporter (lower arm of the six-state scheme) were systematically varied in a binary manner. The substrate luminal affinity ($K_{D,out}$) was adjusted accordingly to meet the microscopic reversibility principle. I–V curves were simulated for the 16 resulting substrates at 20 and 5 mM luminal and cytosolic concentrations, respectively. The heat map shows the intensity of the outward current at +100 mV and the decrease of the inward current by the inner substrate at −50 mV. Substrates 3 and 11 were selected to mimic the Lys-like and Arg-like behaviors, respectively. (*B*) I–V curves of the S3 and S11 currents in a refined uniporter model for the indicated conditions. (*C*) Uniport and exchange cycling frequencies underlying the currents in *B* are shown at −50 mV and +100 mV. (*D*) The model was tested in simulations of a finite reservoir (1 μL) at −50 mV with 5×10^8 transporters. (*E*) Representative single-transporter trajectories with S11 corresponding to the times 0 (*Left*) and 270 s (*Right*) in the reservoir-filling simulations.

gate and by dissociating more slowly from the lumen-facing site (Fig. 7*A*).

The two substrates were characterized further in the initial model and a refined model (*SI Appendix*, Table S1). In zero-*trans* conditions, they induce similar inward and outward currents (Fig. 6*B* and *SI Appendix*, Fig. S4*D*, dashed and dashed-dotted lines). However, when the substrate is present on both sides, the S11 I–V curve stands out through its strong inward rectification (Fig. 6*B* and *SI Appendix*, Fig. S4*D*, solid lines). We quantified uniport and exchange cycles in diverse conditions. Although the presence of S11 in *trans* induced more exchange than S3, this exchange mode remained limited and did not compensate the large decrease of the uniport mode (Fig. 6*C*). S11 is therefore an efficient transinhibitor. In another set of simulations, we assigned a finite volume to the cytosolic compartment and studied the evolution of the loading current during reservoir filling. In agreement with the PQLC2 data, S11 but not S3 loading induced a fast rundown of the loading current, although the two substrates initially accumulate at an identical rate (Fig. 6*D*). Our uniporter model therefore recapitulates many features of PQLC2.

Analysis of the reservoir-filling data showed that the fast rundown induced by S11 tightly correlates with its occupancy of the cytosol-facing site, in contrast with S3 (*SI Appendix*, Fig. S4*E*). We performed single-transporter simulations to understand how S11 binding blocks the uniporter. When the cytosolic reservoir is empty, the uniporter quickly cycles in the inward (counterclockwise) direction as expected (Fig. 6*E*). When the reservoir fills, S11 binds to the cytosol-facing transporter (IN:S state), triggering the cytosolic gate to close (occluded state, Occ:S) because of the high $k^{S}_{i,op}$ value associated with this substrate. Further "backward" (clockwise) progression to the lumen-facing state (OUT:S) is, however, limited by the negative potential. The transporter is therefore trapped into a partial equilibrium between the IN, IN:S, and Occ:S states (Fig. 6*E*, shaded areas), leading to *trans*-inhibition.

It should be noted that this partial equilibrium trap constantly samples substrates from the cytosolic compartment, explaining why cytosolic Arg transinhibits the Lys and His currents (Figs. 4 and 5*D*). At highly negative potential, the positive charge of the substrate opposes cytosolic gate closing. The trap is thus overpowered, narrowing the gap between the S3 and S11 currents (Fig. 6*B*, solid lines). Consistent with this mechanism, the decrease of the PQLC2 inward current by Arg_{in} is stronger at 0 mV than at −100 mV (Fig. 3*H*).

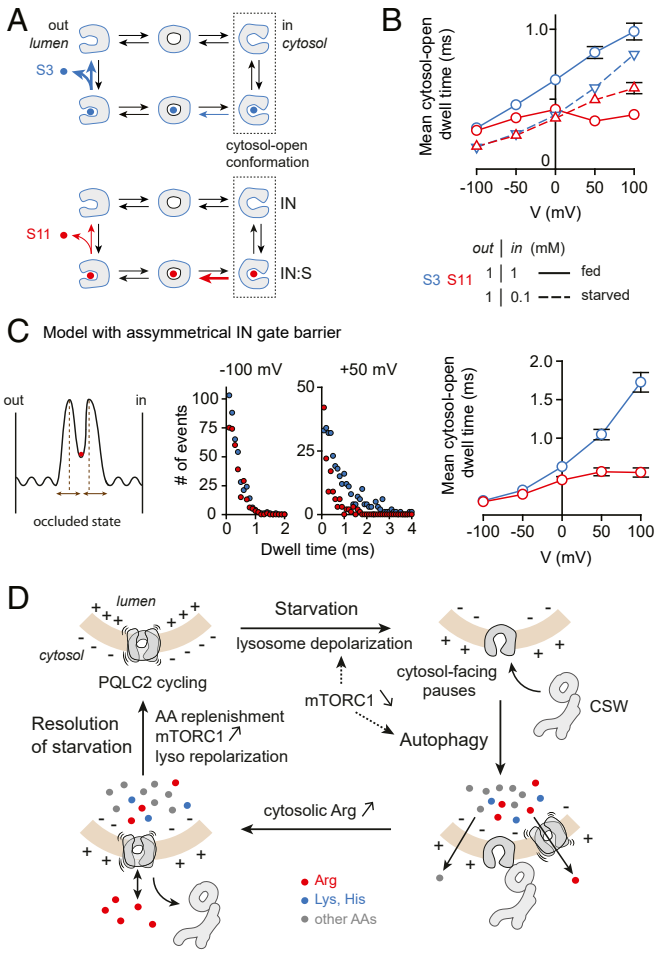

Fig. 7. Lysosomal depolarization and the Arg-like substrate S11 antagonistically control the cytosol-facing conformation. (*A*) Kinetic differences induced by substrates 3 and 11 in the uniporter model. (*B*) The voltage dependence of the dwell time in cytosol-facing conformation was determined from single-transporter simulations in conditions mimicking nutrient replete and starved conditions (cytosolic substrate at 1 and 0.1 mM, respectively). Mean ± SEM of five 200-ms simulations, representing 100 to 750 events per condition. (*C*) Single-transporter simulations were repeated for a uniporter with an asymmetrical energy barrier of the cytosolic gate and otherwise identical model parameters. Dwell time distributions at two potentials and voltage dependence of the mean dwell time in cytosol-facing conformation (60 to 700 events per condition). (*D*) Putative model for the regulation of the interaction between PQLC2 and the CSW complex by the nutrient status. Lysosomal depolarization and cytosolic Arg may antagonistically control this interaction by increasing and shortening the duration of PQLC2 pauses in cytosol-facing conformation.

Altogether, these simulations suggest that the unique interaction of Arg with PQLC2 may arise from its higher affinity for the lumen-facing substrate site and its modulation of the cytosolic gate (faster closing in Arg-bound than Lys- or His-bound state). The latter feature critically explains the fast rundown of the PQLC2 current by cytosolic Arg.

Potential Biological Significance of the Arg Effect. To assess the biological significance of the Arg/PQLC2 interaction, we examined whether S3 and S11 could differentially alter the uniporter state during nutrient starvation and repletion. Starvation predominantly impacts the cytosolic pool of CAAs (3), resulting in a steeper outward concentration gradient across the lysosomal membrane. We thus made single-transporter simulations with a high (1 mM) or low (0.1 mM) cytosolic concentration to mimic fed and starved conditions, respectively. Voltage was also varied because starvation depolarizes the lysosomal membrane, that is, the lysosomal lumen becomes less positive (31–34). Because substrates critically alter cytosolic gating, we focused on the cytosol-facing conformation (fast IN ↔ IN:S equilibrium in Fig. 7*A*).

The dwell time of the cytosol-facing conformation in fed and starved conditions is shown in Fig. 7*B*. In starvation-mimicking conditions, lysosome depolarization increases this dwell time in a similar manner for the two substrates (dashed lines in Fig. 7*B*). However, upon nutrient repletion, the two substrates have diverging effects: S3 stabilizes the cytosol-facing pauses, whereas S11 abrogates these pauses regardless of the membrane potential (solid lines in Fig. 7*B*). This divergence strengthens when the cytosolic gate has an asymmetrical rather than a symmetrical energy barrier (Fig. 7*C*). Lysosomal depolarization and S11 repletion therefore have antagonistic effects on the propensity of the uniporter to pause in cytosol-facing conformation.

These data suggest the following hypothetical model whereby PQLC2 signals the nutrient status to its interaction partners through opposite effects of the lysosomal potential and Arg levels (Fig. 7*D*). Recent in situ measurements in live cells showed that lysosomes have a high membrane potential ($V_{lyso} = V_{cytosol} - V_{lumen} = \sim -100$ mV) in the fed state (33), although in some cell types such as RAW 264.7 macrophages, lysosomes have a lower hyperpolarization (33, 35). Lysosome patch-clamp measurements provided lower or positive values for their membrane potential (31, 32, 36, 37), but this technique uses artificially enlarged lysosomes, and the recorded potential depends on the ionic solution in the micropipette. Upon amino acid starvation, lysosomes depolarize because mTORC1 inactivates and releases its inhibition of TPC and TPRML1 channels (32–34). Our model predicts that this depolarization should induce pauses of PQLC2 in cytosol-facing conformation, a state which would favor recruitment of the CSW complex. In parallel, mTORC1 inactivation induces autophagy, releasing in the organelle lumen amino acids which are exported by lysosomal transporters. The higher luminal affinity of PQLC2 for Arg would favor Arg export over Lys and His export by remaining CSW-free PQLC2 transporters. The resulting local increase in cytosolic Arg would suppress the cytosol-facing pauses of PQLC2, shifting the CSW complex binding equilibrium toward dissociation even though lysosomes are still depolarized. Finally, when autophagy has replenished amino acids, mTORC1 reactivates, and lysosomes return to their hyperpolarized state (Fig. 7*D*). According to this model, two distinct clues, lysosomal depolarization and cytosolic Arg, would be transduced by PQLC2 to signal the nutrient status to the CSW complex at the surface of lysosomes.

Discussion

In this study, we characterized the energetic and kinetic properties of the lysosomal CAA transporter PQLC2. Three approaches, radioactive uptake under voltage clamp, intracellular pH recording, and reversal potential measurements, showed that PQLC2 is uncoupled from lysosomal ion gradients (Figs. 1 and 2). It therefore operates as a uniporter moving CAAs in one direction or the other across the lysosomal membrane depending on the physiological conditions, in contrast with H^+-driven lysosomal transporters. The ability of PQLC2 to reverse is determined by lysosomal [CAA] gradients and the lysosomal potential, which in turn depend on the cell type and nutrient status (3, 33). Arg and Lys fluxes should reverse in an independent manner because PQLC2 has limited exchange activity (Fig. 5*B*). In the case of His, the lysosomal flux is biased toward export because the low fraction of protonated His in the cytosol limits recognition, and import, by PQLC2. Although thermodynamically uncoupled from the H^+ gradient, it should be noted that PQLC2 is kinetically controlled

by the V-ATPase since its transport activity requires an acidic lumen (14).

PQLC2 is also modulated in a selective, intricate manner by Arg levels. Luminal Arg, but not Lys or His, impairs its outward current (Fig. 3), equivalent to lysosomal import, and, conversely, cytosolic Arg selectively decreases its inward current (Fig. 4), equivalent to lysosomal export. Owing to these effects, Arg-evoked I–V curves have a marked concave downward shape that contrasts with the Lys and His curves (Fig. 3 *H* and *I*). Arg and His flux measurements in the oocyte filling paradigm clearly show that these effects are caused by Arg-mediated *trans*-inhibition rather than a greater propensity of Arg to act as a *trans* substrate in exchange reactions (Fig. 5). Arg therefore interacts with PQLC2 in a unique manner that limits its uphill translocation against the electrochemical gradient.

To examine how such paradoxical substrate-yet-inhibitor properties could arise, we modeled the PQLC2 cycle and systematically explored the influence of substrate-dependent rate constants on the current–voltage relationship. Strikingly, only a small subset of cases recapitulated the concave downward aspect of Arg I–V curves, and the differences between the Arg and Lys currents could be recapitulated by a pair of substrates, S3 and S11, differing in just two steps of the transport cycle (Fig. 7*A*). Therefore, a plausible explanation for the unique modulation of PQLC2 by Arg could be the combination of its higher affinity to the lumen-facing site, in agreement with oocyte data (*SI Appendix*, Fig. S3), with its acceleration of cytosolic gate closing compared to the Lys-bound or His-bound transporter (Fig. 7*A*). As the guanidinium group of Arg enables a larger number of electrostatic interactions than Lys or His side chains and can interact in three possible directions (38, 39), these features may reflect Arg-specific PQLC2/substrate interactions that stabilize binding to the lumen-facing site and lower the transition state energy of cytosolic gate closing.

In addition to amino acid transport, PQLC2 has been implicated in an amino acid–sensing pathway, which recruits the CSW complex to lysosomes when CAAs are scarce (21). To assess whether the above properties could participate in this signaling function, we examined the effect of membrane potential and substrate concentrations on the transporter's conformational states in the kinetic model. Because of the differences between S3 and S11, we focused on the cytosol-facing conformation. The dwell time in this conformation is minimal when lysosomes are hyperpolarized, which is their normal state in live cells according to a recent study (33). During amino acid starvation, lysosomal depolarization increases this dwell time because cytosolic gate closing in apo state (the main exit route at low cytosolic concentration) is less favorable at positive potentials. However, when depolarized lysosomes are exposed to higher cytosolic concentrations, the Arg-like (S11), but not the Lys-like (S3), substrate shortens the cytosol-facing pauses (Fig. 7 *B* and *C*), owing to its specific effect on the cytosolic gate.

These simulation data lead us to propose a model for the amino acid–sensing function of PQLC2 in which the transporter recruits the CSW complex in a cytosol-facing conformation and in which lysosomal depolarization and cytosolic Arg are antagonistic clues sensed by the complex to signal amino acid starvation and repletion, respectively (Fig. 7*D*). Interestingly, an independent study recently provided homology modeling and biochemical evidence for an interaction of PQLC2 in its cytosol-facing conformation with the WDR41 subunit of the complex (40). Further studies should tell whether this interaction is modulated by the lysosomal potential and by Arg, rather than Lys and His, as our model predicts.

Another feature of our model deserving experimental exploration is the prediction that the CSW recruitment cycle is nested within the mTORC1 cycle: the CSW complex would be recruited to lysosomes in response to a signal (lysosomal depolarization) induced by mTORC1 inactivation, while it would eventually be released from lysosomes by cytosolic Arg before mTORC1 reactivates. The bidirectionality of PQLC2 could strengthen this temporal relationship between the CSW and mTORC1 cycles: when lysosomes freed from the CSW complex are still depolarized, PQLC2 reversal and lysosomal Arg import could help in reactivating mTORC1 by increasing luminal Arg levels to upregulate the luminal Arg sensor SNAT9.

Materials and Methods

Solutions and Reagents. Oocyte recordings were performed in ND100 medium (100 mM NaCl, 2 mM KCl, 1 mM $MgCl_2$, and 1.8 mM $CaCl_2$) buffered with 5 mM 2-(*N*-morpholino)ethanesulfonic acid (MES)-NaOH to pH 5.00, unless stated otherwise. L-Arg, L-Lys, or L-His (Sigma-Aldrich) were added as monohydrochloride salts. For substrate-free solutions, the amino acid was replaced by NMDG hydrochloride (Sigma-Aldrich) to keep the chloride concentration and osmolarity unchanged. The maximum concentration of NMDG used (20 mM) had no effect on PQCL2 and endogenous currents. For patch-clamp recordings in HEK293T cells, the substrate-free external solution contained the following: 130 mM NaCl, 5 mM KCl, 2 mM $CaCl_2$, 1 mM $MgCl_2$, 20 mM glucose, 20 mM NMDG-Cl, and 20 mM MES adjusted to pH 5.00 with NaOH or HCl (osmolarity: 315 to 330 mOsm). For substrate application, NMDG was replaced by 20 mM Lys, Arg, or His. The micropipette solution contained the following: 130 mM CsCl, 10 mM ethylene glycol-bis(β-aminoethyl ether)-N,N,N′,N′-tetraacetic acid (EGTA), 2 mM CaCl2, 2 mM MgCl2, and 10 mM Hepes adjusted to pH 7.35 to 7.40 with KOH or HCl, supplemented with 20 mM NMDG, Arg, or Lys (osmolarity: 295 to 305 mOsm). L-[2,3,4-^{3}H]arginine monhydrochloride (specific activity: 40 to 50 Ci/mmol) was from Perkin-Elmer.

Expression in *Xenopus* Oocytes. The care and use of animals were performed according to local and national guidelines (Project Authorization for the Use of Animals for Scientific Purposes agreement no. 14316) in compliance with the European Animal Welfare regulations and Home Office regulations (United Kingdom). *Xenopus laevis* oocytes were prepared as described (17). Defolliculated oocytes were injected with 50 ng complementary RNA (1 μg/μL) coding for an EGFP-tagged, sorting mutant of PQLC2 (PQLC2-LL290/291AA-EGFP) to express the transporter at the plasma membrane (14). Between 24 to 48 h after injection, PQLC2-expressing oocytes were selected under an Eclipse TE-2000 epifluorescence microscope (Nikon) or an Axiophot epifluorescence microscope (Zeiss). Oocytes injected with 50 nL water were used as negative control.

Two-Electrode Voltage Clamp Recording in *Xenopus* Oocytes. Recordings were done at room temperature with two borosilicate-glass Ag/AgCl microelectrodes filled with 3 M KCl (0.5 to 3 MΩ tip resistance) connected to an O725C amplifier (Warner Instrument) and a Digidata 1440A interface controlled via pCLAMP 10.7 software (Molecular Devices). Oocytes were preincubated ≥30 min in ND100 pH 5.00 to activate PQLC2 (14) and lower their CAA contents by PQLC2 reversal. An Ag/AgCl reference electrode was positioned near the oocyte. When different chloride concentrations were used, the Ag/AgCl electrode was separated from the perfusion chamber using a salt bridge filled with 1.5 M KCl and 2% agar agar. In low chloride conditions (Fig. 2*E*), a +6 mV correction was applied to V_{rev} to compensate for the liquid junction potential at the tip of the salt bridge. Currents recorded at constant voltage were filtered using a 10-Hz low-pass filter and sampled at 1 kHz. For voltage jump experiments, currents were filtered at 0.5 kHz and sampled at 5 kHz. Voltage steps were applied from +100 to −100 mV with −20 mV decrements. To minimize the endogenous depolarization-induced conductance, oocytes were held at −20 mV and the holding potential was set to −40 mV for 100 ms just before and after each step. Data were analyzed with Clampfit 10.7 (Molecular Devices). Charge–substrate ratio, reversal potential, and pH_{in} measurements are described in *SI Appendix, Supplementary Methods*.

Kinetic Modeling. PQLC2 kinetics were modeled using a six-state model (*SI Appendix*, Fig. S4*A*). Voltage dependence was implemented according to Läuger and Rauch (41), with symmetrical energy barriers unless stated otherwise (see rate constant equations detailed in *SI Appendix, Supplementary Methods*). The numerical values used in the simulations are provided in *SI Appendix*, Table S1. Briefly, substrate affinities were set in the millimolar range with an association limited by diffusion. Gating rate constants were in the millisecond time range, with faster kinetics in apo- than loaded-state transitions to account for the limited exchange activity of PQLC2 (Fig. 5). Voltage-dependence parameters were defined after a preliminary systematic study of their impact on I–V curves (*SI Appendix*, Fig. S4*B*). A total charge

($\eta + \theta$) displaced close to −0.5 during apo-state transitions proved critical to recapitulate the monotonic aspect of PQLC2 I-V curves. Indeed, this value allows the membrane potential to drive both the apo and loaded arms of the transport cycle, avoiding the emergence of a rate-limiting step over a large voltage range.

Steady-state currents, cycling frequencies, and single-transporter trajectories were simulated with the MarkovEditor software (https://github.com/mikpusch/MarkovEditor). To detect exchange cycles, we duplicated the loaded arm of the model and divided by two the rate constant of split transitions (*SI Appendix*, Fig. S4*F*). The exchange is displayed by selecting the largest eight-state loop in the "select cycle" function of MarkovEditor: the plot provides half the exchange rate as a function of voltage, while each six-state loop provides half the uniport rate. For reservoir filling, we used 5×10^8 transporters with a cytosolic volume of 1 μL and divided rate constants by a scaling factor (5,000) to speed up simulations. Single-transporter stochastic simulations were repeated five times for 200 ms for each condition. To avoid sampling issues, the full sequences of states over time were recovered and transferred into Excel. A macro was used to detect each IN ↔ IN:S equilibrium event (cytosol-facing conformation) and determine their dwell time.

Statistical Analysis. A two-tailed Mann–Whitney *U* test was used for comparison between two groups and a one-way ANOVA with Tukey post hoc test for multiple groups. Error bars represent SEM.

Reference *SI Appendix, Supplementary Methods* for other techniques.

Data Availability. All study data are included in the article and/or *SI Appendix*.

ACKNOWLEDGMENTS. We thank Philippe Ascher and the late JacSue Kehoe for helpful advice. We thank the animal facility and the prototyping facility of Unité Mixte de Service BioMedTech facilities at Université de Paris (CNRS UMS2009, INSERM US36) for housing the frogs and for making a microelectrode rack. This work was supported by the Cystinosis Research Foundation (Grant Nos. CRFS-2014-004 and CRFF-2016-005 to B.G.) and by the French Agence Nationale de la Recherche (ANR) (Grant No. ANR-18-CE11-0009-01 to B.G.).

1. A. Ballabio, J. S. Bonifacino, Lysosomes as dynamic regulators of cell and organismal homeostasis. *Nat. Rev. Mol. Cell Biol.* **21**, 101–118 (2019).
2. Q. Verdon *et al*., SNAT7 is the primary lysosomal glutamine exporter required for extracellular protein-dependent growth of cancer cells. *Proc. Natl. Acad. Sci. U.S.A.* **114**, E3602–E3611 (2017).
3. G. A. Wyant *et al*., mTORC1 activator SLC38A9 is required to efflux essential amino acids from lysosomes and use protein as a nutrient. *Cell* **171**, 642–654.e12 (2017).
4. K. J. Condon, D.M. Sabatini, Nutrient regulation of mTORC1 at a glance. *J. Cell Sci.* **132**, jcs222570 (2019).
5. R. E. Lawrence, R. Zoncu, The lysosome as a cellular centre for signalling, metabolism and quality control. *Nat. Cell Biol.* **21**, 133–142 (2019).
6. R. L. Wolfson, D. M. Sabatini, The dawn of the age of amino acid sensors for the mTORC1 pathway. *Cell Metab.* **26**, 301–309 (2017).
7. M. Rebsamen *et al*., SLC38A9 is a component of the lysosomal amino acid sensing machinery that controls mTORC1. *Nature* **519**, 477–481 (2015).
8. B. M. Castellano *et al*., Lysosomal cholesterol activates mTORC1 via an SLC38A9-Niemann-Pick C1 signaling complex. *Science* **355**, 1306–1311 (2017).
9. S. Wang *et al*., Metabolism. Lysosomal amino acid transporter SLC38A9 signals arginine sufficiency to mTORC1. *Science* **347**, 188–194 (2015).
10. J. Jung, H. M. Genau, C. Behrends, Amino acid-dependent mTORC1 regulation by the lysosomal membrane protein SLC38A9. *Mol. Cell. Biol.* **35**, 2479–2494 (2015).
11. S. A. Fromm, R. E. Lawrence, J. H. Hurley, Structural mechanism for amino acid-dependent Rag GTPase nucleotide state switching by SLC38A9. *Nat. Struct. Mol. Biol.* **27**, 1017–1023 (2020).
12. H. T. Lei, J. Ma, S. Sanchez Martinez, T. Gonen, Crystal structure of arginine-bound lysosomal transporter SLC38A9 in the cytosol-open state. *Nat. Struct. Mol. Biol.* **25**, 522–527 (2018).
13. B. Liu, H. Du, R. Rutkowski, A. Gartner, X. Wang, LAAT-1 is the lysosomal lysine/arginine transporter that maintains amino acid homeostasis. *Science* **337**, 351–354 (2012).
14. A. Jézégou *et al*., Heptahelical protein PQLC2 is a lysosomal cationic amino acid exporter underlying the action of cysteamine in cystinosis therapy. *Proc. Natl. Acad. Sci. U.S.A.* **109**, E3434–E3443 (2012).
15. P. Kandasamy, G. Gyimesi, Y. Kanai, M. A. Hediger, Amino acid transporters revisited: New views in health and disease. *Trends Biochem. Sci.* **43**, 752–789 (2018).
16. M. Town *et al*., A novel gene encoding an integral membrane protein is mutated in nephropathic cystinosis. *Nat. Genet.* **18**, 319–324 (1998).
17. R. Ruivo *et al*., Mechanism of proton/substrate coupling in the heptahelical lysosomal transporter cystinosin. *Proc. Natl. Acad. Sci. U.S.A.* **109**, E210–E217 (2012).
18. M. Huizing, W. A. Gahl, Inherited disorders of lysosomal membrane transporters. *Biochim. Biophys. Acta Biomembr.* **1862**, 183336 (2020).
19. L. Feng, W. B. Frommer, Evolution of transporters: The relationship of SWEETs, PQ-loop, and PnuC transporters. *Trends Biochem. Sci.* **41**, 118–119 (2016).
20. S. Newstead, F. Barr, Molecular basis for KDEL-mediated retrieval of escaped ER-resident proteins – SWEET talking the COPs. *J. Cell Sci.* **133**, jcs250100 (2020).
21. J. Amick, A. K. Tharkeshwar, G. Talaia, S. M. Ferguson, PQLC2 recruits the C9orf72 complex to lysosomes in response to cationic amino acid starvation. *J. Cell Biol.* **219**, e201906076 (2020).
22. R. Higuchi-Sanabria *et al*., Lysosomal recycling of amino acids affects ER quality control. *Sci. Adv.* **6**, eaaz9805 (2020).
23. J. G. O'Rourke *et al*., C9orf72 is required for proper macrophage and microglial function in mice. *Science* **351**, 1324–1329 (2016).
24. R. Sivadasan *et al*., C9ORF72 interaction with cofilin modulates actin dynamics in motor neurons. *Nat. Neurosci.* **19**, 1610–1618 (2016).
25. W. McAlpine *et al*., Excessive endosomal TLR signaling causes inflammatory disease in mice with defective SMCR8-WDR41-C9ORF72 complex function. *Proc. Natl. Acad. Sci. U.S.A.* **115**, E11523–E11531 (2018).
26. J. Amick, S. M. Ferguson, C9orf72: At the intersection of lysosome cell biology and neurodegenerative disease. *Traffic* **18**, 267–276 (2017).
27. D. Tang *et al*., Cryo-EM structure of C9ORF72-SMCR8-WDR41 reveals the role as a GAP for Rab8a and Rab11a. *Proc. Natl. Acad. Sci. U.S.A.* **117**, 9876–9883 (2020).
28. M. Y. Su, S. A. Fromm, R. Zoncu, J. H. Hurley, Structure of the C9orf72 ARF GAP complex that is haploinsufficient in ALS and FTD. *Nature* **585**, 251–255 (2020).
29. P. Morin, C. Sagné, B. Gasnier, Functional characterization of wild-type and mutant human sialin. *EMBO J.* **23**, 4560–4570 (2004).
30. N. R. Latorraca *et al*., Mechanism of substrate translocation in an alternating access transporter. *Cell* **169**, 96–107.e12 (2017).
31. H. Xu, D. Ren, Lysosomal physiology. *Annu. Rev. Physiol.* **77**, 57–80 (2015).
32. C. Cang *et al*., mTOR regulates lysosomal ATP-sensitive two-pore Na(+) channels to adapt to metabolic state. *Cell* **152**, 778–790 (2013).
33. A. Saminathan *et al*., A DNA-based voltmeter for organelles. *Nat. Nanotechnol.* **16**, 96–103 (2020).
34. D. L. Medina *et al*., Lysosomal calcium signalling regulates autophagy through calcineurin and TFEB. *Nat. Cell Biol.* **17**, 288–299 (2015).
35. M. Koivusalo, B. E. Steinberg, D. Mason, S. Grinstein, In situ measurement of the electrical potential across the lysosomal membrane using FRET. *Traffic* **12**, 972–982 (2011).
36. Q. Cao *et al*., BK channels alleviate lysosomal storage diseases by providing positive feedback regulation of lysosomal Ca^{2+} release. *Dev. Cell* **33**, 427–441 (2015).
37. W. Wang *et al*., A voltage-dependent K^+ channel in the lysosome is required for refilling lysosomal Ca^{2+} stores. *J. Cell Biol.* **216**, 1715–1730 (2017).
38. B. Musafia, V. Buchner, D. Arad, Complex salt bridges in proteins: Statistical analysis of structure and function. *J. Mol. Biol.* **254**, 761–770 (1995).
39. R. Ferreira de Freitas, M. Schapira, A systematic analysis of atomic protein-ligand interactions in the PDB. *MedChemComm* **8**, 1970–1981 (2017).
40. G. Talaia, J. Amick, S. M. Ferguson, Receptor-like role for PQLC2 amino acid transporter in the lysosomal sensing of cationic amino acids. *Proc. Natl. Acad. Sci. U.S.A.* **118**, e2014941118 (2021).
41. P. Läuger, P. Jauch, Microscopic description of voltage effects on ion-driven cotransport systems. *J. Membr. Biol.* **91**, 275–284 (1986).